scientific reports

Check for updates

OPEN

A novel electrocardiogram-synchronized laser Doppler holography system for cardiac cycle-resolved retinal hemodynamics: development and validation

Keren Wood[1,2], Nicholas Schnorbus[3], Luis Muncharaz[2], Yash Lahoti[1], Brent A. Siesky[1], Giovanna Guidoboni[4], Alice Verticchio Vercellin[1], Samuel Potash[1], Lily A. Greenberg[2], Michael Atlan[5], Toco Y. P. Chui[2], Richard Rosen[2] & Alon Harris[1]✉

The retinal microvasculature is one of the few sites where the microcirculation can be directly and non-invasively visualized in vivo, offering a unique window into ocular disease and systemic health. In this study we developed and validated a novel imaging platform integrating a custom-built one-lead electrocardiogram (ECG) with laser Doppler holography (LDH), a high-speed imaging technique that captures Doppler-induced phase shifts, for real-time cardiac cycle-resolved assessment of retinal hemodynamics. Twenty-five healthy adults were imaged (five images per eye), with 563 cardiac cycles meeting analysis quality criteria. Internal system latency combined with synchronization offset amounted to less than 5 ms. LDH-derived beat-to-beat intervals closely tracked ECG R-R intervals, with small mean differences (~ 3 ms), demonstrating excellent temporal stability without measurable drift. ECG-retina latencies, defined as time from the ECG R-peak to LDH peak systolic velocity (R-PSV), maximal systolic upslope (R-MaxSlope), and 50% PSV amplitude (R-PSV½), were measured. R-PSV½ mean ± SD was 128 ± 18 ms and showed the highest repeatability (ICC = 0.78, median CV = 4.8%). ECG-retina latencies were moderately associated with age and heart rate, in exploratory analyses. This integrated ECG-LDH platform provides repeatable, synchronized, high-speed, cardiac-resolved retinal hemodynamic measurements and establishes a quantitative framework for studying the eye-heart relationship.

Keywords Laser Doppler holography, Retinal hemodynamics, Oculomics, Method validation, Electrocardiography, Synchronization

Retinal vessels share structural and functional characteristics with systemic and central nervous system microvasculature[1–4]. Due to their anatomical features, they provide a unique opportunity to directly and non-invasively visualize the microcirculation in vivo, offering an unparalleled window into both ocular disease and systemic health[1,2,5]. Measuring blood flow changes can advance our understanding of ocular physiology and pathophysiology with impaired blood flow being linked to many ocular conditions, including glaucoma, diabetic retinopathy and age-related macular degeneration[6–13]. Beyond ophthalmology, these accessible retinal features are increasingly recognized as a potential source for biomarkers of systemic health - helping drive the

[1]Department of Ophthalmology, Icahn School of Medicine at Mount Sinai, Annenberg 22-86, 1468 Madison Avenue, Box 1183, New York, NY 10029, USA. [2]New York Eye and Ear Infirmary of Mount Sinai, New York, NY, USA. [3]Rensselaer Polytechnic Institute, Troy, NY, USA. [4]Maine College of Engineering and Computing, University of Maine, Orono, ME, USA. [5]Langevin Institute, French National Centre for Scientific Research (CNRS), Paris Sciences & Letters University (PSL), ESPCI Paris (École Supérieure de Physique et de Chimie Industrielles), Paris, France. ✉email: alon.harris@mssm.edu

field of Oculomics, where ocular images serve as a non-invasive window to systemic disease, with findings in cardiovascular and metabolic disorders, neurodegenerative conditions such as Alzheimer's disease and Parkinson's disease, multiple sclerosis, among others[14–21].

While several imaging modalities exist to characterize ocular blood flow, they each have their limitations. Color Doppler imaging (CDI) measures real time flow in the larger retrobulbar vessels supplying the eye, however the technique is operator-dependent, lacks spatial resolution for imaging smaller vessels and typically requires manual measurement of output parameters[22,23]. Optical coherence tomography angiography (OCTA) provides high-resolution detailed maps of retinal and choroidal vasculature, but lacks dynamic, temporal information[24,25]. Conversely, laser speckle offers temporal resolution of retinal blood flow, but is limited by noise, relatively low spatial resolution and conventional methods provide only relative perfusion, though recent approaches can estimate flow velocity more directly[26].

Laser Doppler holography (LDH) is a new imaging device that provides full-field, high-speed assessment of retinal blood flow by capturing Doppler-induced phase changes in holographic recordings of backscattered laser light[27–30]. The device records 3.5-second videos and outputs extensive data including arterial and venous velocities, waveform morphology throughout the cardiac cycle, resistivity and pulsatility index, among other derived metrics (Fig. 1). Because retinal blood flow is inherently pulsatile and exhibits characteristics of the cardiac cycle - coupling LDH to an electrocardiogram (ECG) would allow for alignment of flow pulses to the cardiac cycle to enable cardiac cycle-resolved hemodynamic analysis. ECG-based alignment has the potential to also provide a common temporal reference to synchronize LDH data with other ECG-gated modalities, including echocardiography, even if acquisitions are performed on different days or in different locations - providing a reliable key for cross-modality alignment.

This study presents a novel custom-built one-lead ECG system synchronized and integrated into an LDH device for real-time hemodynamic assessment. We demonstrate the feasibility and repeatability of this system, providing a proof-of-concept for the eye-heart hemodynamic axis and laying the foundation for future studies exploring the relationship between ocular blood flow and systemic vascular health.

Methods

Study population

This study was a prospective cross-sectional observational study conducted in the New York Eye and Ear Infirmary of Mount Sinai, New York, New York, United States. The study was conducted in accordance with the Declaration of Helsinki and the study protocol was approved by the Institutional Review Board of Icahn School of Medicine at Mount Sinai, New York, NY, USA (protocol code: STUDY-24-01722; date of approval: February 12th, 2025). A written informed consent was signed by all study subjects before the start of this study.

Twenty-five healthy adults (≥ 18 years) with no ocular or uncontrolled systemic disease were recruited and imaged between October and November 2025 and were imaged on the LDH device integrated with our custom one-lead ECG.

System design

ECG data was acquired using a custom-built single lead recording system based on an Arduino Nano microcontroller and a SparkFun AD8232 heart rate monitor breakout board. The AD8232 provided analog amplification and filtering for a simple three electrode, single lead ECG configuration. The Arduino Nano's analog-to-digital converter sampling rate was set to 500 Hz (every 2 ms), providing adequate temporal resolution

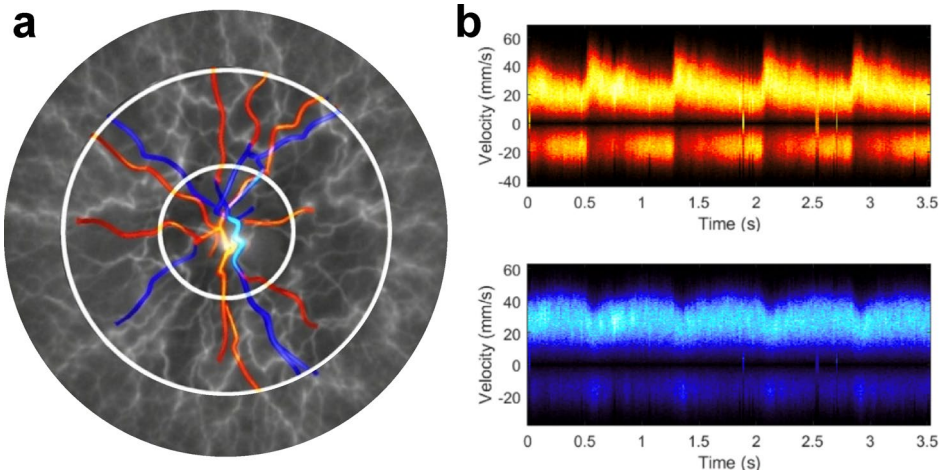

Fig. 1. Representative laser Doppler holography (LDH) output. (**a**) LDH image showing the optic nerve head with segmented retinal vessels (arteries in orange, veins in blue). To protect biometric privacy, the vascular architecture has been synthetically modified using AI. (**b**) Velocity spectrograms (mm/s) over the 3.5-second acquisition in the arteries (top, orange) and veins (bottom, blue), showing pulsatile waveform morphology.

to capture cardiac features such as the QRS complex while allowing stable real-time data acquisition. The ECG system was used alongside the LDH setup, allowing concurrent acquisition.

At the start of each scan, the LDH system recorded a single Unix timestamp, derived from the host computer's nanosecond-resolution clock. Simultaneously, the ECG continuously recorded time points with nanosecond-resolution Unix timestamps from the same host computer. During post-processing, the LDH start timestamp was aligned with the closest ECG timestamp, and the offset was quantified across all scans by subtracting the LDH start timestamp from the corresponding ECG timestamp, yielding an average synchronization offset of 1.17 ± 1.88 ms. This offset was not corrected in post-processing to preserve native acquisition timing and avoid introducing artificial temporal shifts.

Image acquisition and feature extraction

Each participant underwent ECG recording with simultaneous LDH imaging of both eyes, with each eye imaged five times during a single session. Blood pressure (BP) and intraocular pressure (IOP) were measured on the same day, just before imaging. LDH data were acquired using Holovibes v14.11.12. The LDH camera has an acquisition frame rate of 37 kHz (0.03 ms). Each LDH recording lasted 3.5 s, reflecting the default acquisition duration of the current device. Doppler image reconstruction uses a Short-Time Fourier Transform (STFT) with a window size of 512 samples and a window stride of 512 samples (no overlap), resulting in an effective frame rate of 72.3 Hz (13.83 ms) for the reconstructed Doppler images. Doppler hologram rendering was performed with HoloDoppler v2.9.8, and downstream LDH signal analysis with EyeFlow v2.9.10.2.

Custom software was used to align the ECG and LDH signals (Fig. 2A). Because blood flow can show different waveform patterns, such as a delayed peak after a plateau or the presence of multiple peaks, relying on peak timing can be inconsistent[31]. For this reason, when analyzing the LDH signal we not only evaluated peak systolic velocity (PSV), the time of maximum velocity during systole, but also defined two additional timing markers: (1) MaxSlope - point of maximal velocity increase (maximum dv/dt) during the systolic upstroke, and (2) PSV½ - the point at which the systolic upstroke reaches 50% of the pulse amplitude, where pulse amplitude is defined as the difference between the PSV and the preceding diastolic minimum. These provide alternative timing markers that are less directly affected by variations in peak morphology. MaxSlope and PSV½ were calculated from the reconstructed LDH waveform via interpolation, allowing sub-frame interpolation of waveform features. However, the effective temporal resolution of the reconstructed LDH signal remains 13.83 ms. Accordingly, temporal values were derived from interpolation-based (sub-frame) estimates, however they are reported

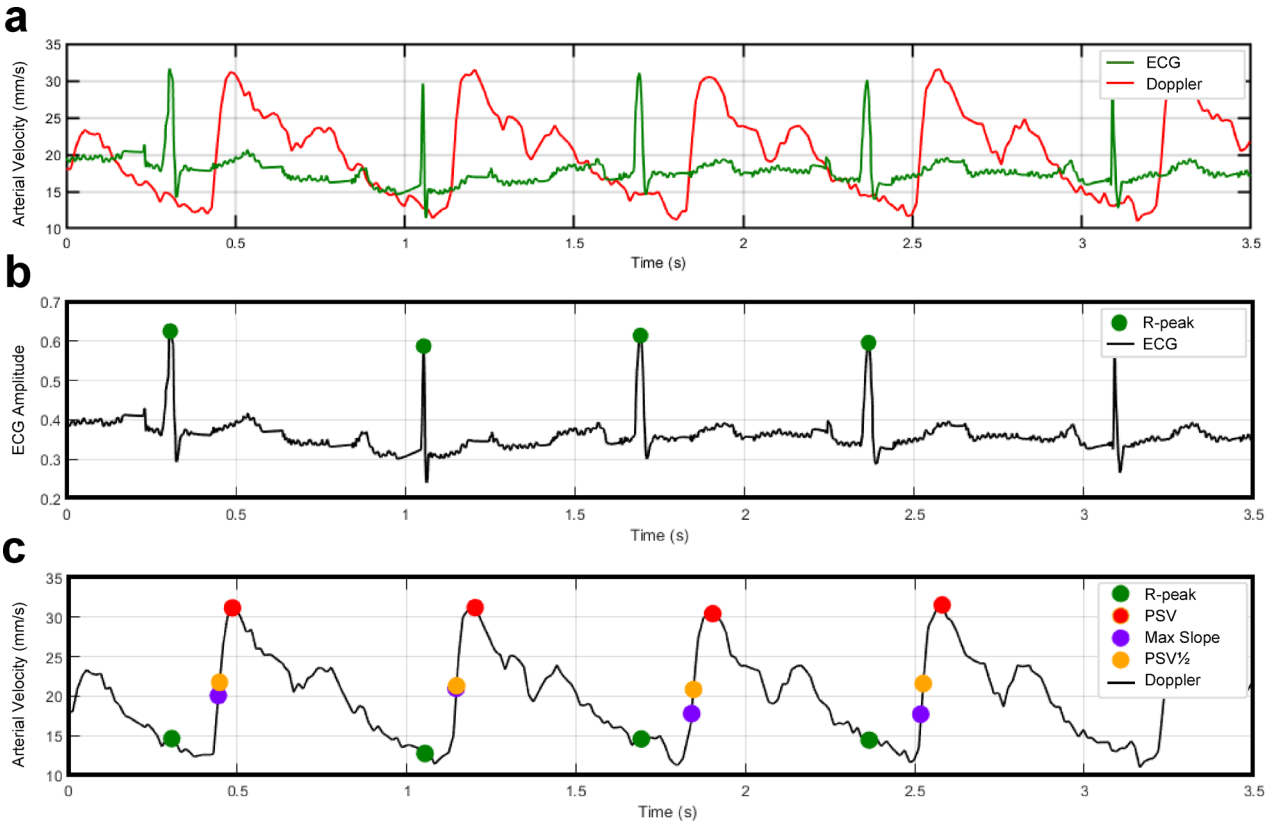

Fig. 2. Signal synchronization and hemodynamic feature extraction. (**a**) 3.5-second trace of the synchronized electrocardiogram (ECG) and laser Doppler holography (LDH) signals. (**b**) Automated detection of ECG R-peaks (green). (**c**) Automated detection of LDH metrics for each cardiac cycle: peak systolic velocity (PSV, red), maximal systolic upslope (MaxSlope, purple), and 50% PSV amplitude (PSV½, orange).

rounded up to the nearest millisecond to avoid overstating precision relative to the underlying signal resolution. Feature extraction and calculation of all temporal parameters were performed using fully automated custom MATLAB scripts (version R2021b; MathWorks, Natick, MA, USA); R-wave peaks were detected from the ECG, LDH metrics were extracted for each cardiac cycle, and intervals and latencies (described below) were computed (Fig. 2B,C). All acquisitions and software-derived outputs underwent a predefined manual quality control review by a single grader (KW). Images or waveforms were excluded if the optic nerve was poorly centered, vessel segmentation was inaccurate, image clarity or registration was insufficient, or if selected waveforms were noisy, affected by motion artifacts, or did not include a complete cardiac cycle. Automated feature detection was also manually verified to ensure correct identification of R-wave peaks and LDH metrics within the same cardiac cycle.

Statistical analysis

To quantify the variability of each system, intervals within the same image were averaged to obtain an image-level average. Averages from different images from the same eye in the same participant were then compared to derive the coefficient of variation (CV) for the ECG and for the LDH intervals, and median CVs were reported.

ECG-LDH temporal stability

To verify the temporal stability between the ECG and the holography systems, we compared ECG R-R intervals to LDH PSV, MaxSlope and PSV½ beat-to-beat intervals. For an interval to be included in the analysis, both beats forming the interval must have passed the manual quality control.

Difference between the LDH and ECG beat-to-beat intervals (LDH minus ECG) was calculated for each interval and analyzed with Bland-Altman, reporting the mean difference (bias) ± SD, the 95% confidence interval (CI) of the mean, and the 95% limits of agreement (LoA; calculated as the mean difference ± 1.96 SD). Statistical significance of the mean differences was assessed using a one-sample t-test against zero. Due to the paired nature of LDH and ECG intervals, physiologic beat-to-beat variability affects both signals equally; consequently, the differences observed in the beat-level analysis should primarily reflect measurement error.

Repeatability of ECG-retina latencies

Latency from the ECG R-peak to each LDH metric (PSV, MaxSlope, PSV½) was computed (R-PSV, R-MaxSlope, R-PSV½). Beat-level values for each of the latencies were averaged for each image, defined as the image-level mean, and then averaged across all images within each eye, defined as the eye-level mean, to calculate between-eye summary statistics. All available beats within each image were included, with the number of analyzable beats per image varying across acquisitions. Image-level and eye-level values were computed as simple (unweighted) means, so that each image contributed equally, maintaining the image as the unit of repeatability. Within-eye repeatability was quantified using the intraclass correlation coefficient [ICC (1,1)] and within-eye variability was assessed with the CV and reported as the median CV across eyes, both from image-level data; a beat-to-beat approach was avoided as it would capture physiologic beat-to-beat variability rather than repeatability of the imaging.

Physiological associations

Differences between the eyes were assessed with paired Wilcoxon signed-rank tests, with right and left eye measurements treated as paired observations within each participant. Sex differences were assessed using Wilcoxon rank-sum tests applied to subject-level eye-averaged parameters. Spearman rank correlations were used to assess relationships between systemic and retinal parameters, with a single value per subject (right and left eye measurements were averaged). Spearman correlations were used rather than Pearson correlations because several variables were not normally distributed. $p < 0.05$ were considered statistically significant.

All statistical analyses were performed using R version 4.5.1 (R Foundation for Statistical Computing, Vienna, Austria).

Temporal variables are reported in milliseconds and rounded up to the nearest integer to reflect the effective temporal resolution (13.83 ms) of the reconstructed LDH signal, whereas hemodynamic amplitude measures are reported with native computational precision.

To protect participants biometric privacy, the vascular architecture in the representative LDH image (Fig. 1A) was synthetically modified using ChatGPT (version ChatGPT-4o, OpenAI, San Francisco, CA; accessed January 7, 2026). The corresponding hemodynamic data (Fig. 1B) remains unaltered.

Results

25 participants (50 eyes) were imaged, with 774 cardiac cycles identified. After quality control, 563 beats remained for analysis. Demographic and hemodynamic variables are summarized in Table 1.

For the entire cohort, ECG R-R interval variability was low with a median CV of 3.4%. LDH-derived beat-to-beat intervals showed median CVs of 4.5% for the PSV-interval, 4.2% for the MaxSlope-interval and 4.2% for the PSV½-interval. These findings indicate minimal variability for both systems, with ECG showing a slightly lower variability.

ECG-LDH temporal stability

From the 563 beats included in the analysis, there were 333 beat-to-beat intervals that met the interval inclusion criteria.

The mean ECG R-R interval was 761 ± 14 ms. Differences between the LDH and the ECG beat-to-beat intervals were small for all three metrics (2–4 ms), corresponding to < 0.5% of the average R-R interval (Table 2). The PSV-interval mean difference approached statistical significance and showed relatively wide LoA. In

	Median (Q_1, Q_3)
Age (years)	32 ± 14*
Sex	12 F (48%), 13 M (52%)
Systolic BP (mmHg)	121 (107, 130)
Diastolic BP (mmHg)	78 (74, 82)
Heart rate (bpm)	76 (70, 81)
MAP† (mmHg)	95 (85, 98)
IOP (mmHg)	
OD	16.7 (14.5, 18.2)
OS	16.3 (14.0, 19.7)
Mean OPP‡ (mmHg)	
OD	46.9 (38.7, 48.4)
OS	46.3 (40.6, 50.1)

Table 1. Demographic and hemodynamic characteristics of the study cohort ($N = 25$). Data are presented as median (Q1, Q3) unless otherwise specified. Q1, Q3 = first, third quartile; BP = blood pressure; MAP = mean arterial pressure; IOP = intraocular pressure; OD = right eye (*oculus dexter*); OS = left eye (*oculus sinister*); OPP = ocular perfusion pressure; *Reported as Mean±standard deviation; †MAP = DBP + 1/3(SBP - DBP); ‡Mean OPP = 2/3MAP-IOP.

Metric	Mean interval (ms)	Mean difference (LDH-ECG) ± SD (ms)	95% CI of the mean difference (ms)	Limits of agreement (ms)	p-value
PSV-interval	765	4 ± 36	0–8	-66-74	0.051
MaxSlope-interval	764	2 ± 21	0–4	-39-44	0.048
PSV½-interval	764	3 ± 21	1–5	-38-43	0.011

Table 2. Bland-Altman agreement between LDH-derived beat-to-beat intervals and ECG R-R intervals. Comparison of beat-to-beat intervals ($n = 333$) of ECG R-R and LDH-derived timing metrics. LDH = laser Doppler holography; ECG = electrocardiogram; SD = standard deviation; CI = confidence interval; PSV = peak systolic velocity; MaxSlope = maximal systolic upslope; PSV½ = 50% PSV amplitude.

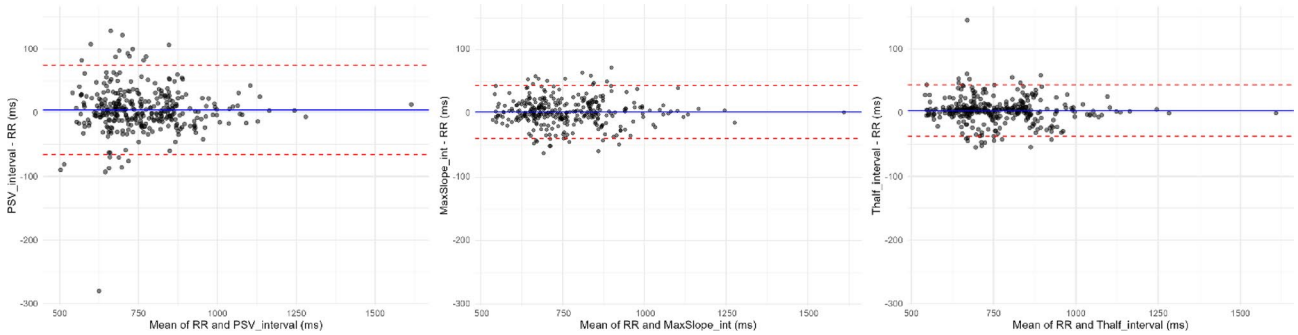

Fig. 3. Bland-Altman plots comparing laser Doppler holography (LDH)-intervals to ECG-intervals. Agreement between ECG R-R intervals and the three LDH timing metrics intervals: peak systolic velocity (PSV, left), maximal systolic upslope (MaxSlope, center), and 50% PSV amplitude (PSV½, right). The blue lines represent the mean difference (bias) between the laser LDH and the ECG. The dashed red lines represent the 95% limits of agreement (LoA). All three metrics show minimal systematic bias, with mean differences around 3 ms. PSV½-interval and MaxSlope-interval showed narrower LoA and tighter clustering of points around the mean, indicating a closer agreement with R-R, compared to the PSV-interval.

contrast, the MaxSlope- and PSV½-intervals showed statistically significant mean differences from ECG timing, but with narrower LoAs (Table 2; Fig. 3).

Repeatability of ECG-retina latencies

Mean ± SD, ICC and median CV for PSV amplitude and the three ECG-retina latencies are summarized in Table 3. ICC values ranged from moderate to strong (0.65–0.78), with median CVs ranging 4.8-6.0%, indicating good repeatability for all metrics. R-PSV½ had the best results for both ICC and CV.

Metric	Mean ± SD, across eyes	ICC	Median CV (%)
PSV amplitude (mm/s)	27.05 ± 3.41	0.75	5.2
R-PSV (ms)	181 ± 26	0.65	5.8
R-MaxSlope (ms)	126 ± 23	0.75	5.6
R-PSV½ (ms)	128 ± 18	0.78	4.8

Table 3. Repeatability of LDH PSV amplitude and ECG-retina latencies. Mean values and repeatability metrics for PSV amplitude and R-peak to LDH timing latencies. SD = standard deviation; ICC = intraclass correlation coefficient (1,1); CV = coefficient of variation; PSV = peak systolic velocity; R-PSV = time from ECG R-peak to PSV; R-MaxSlope = time from ECG R-peak to maximal systolic upslope; R-PSV½ = time from ECG R-peak to 50% PSV amplitude.

Physiological associations

Mean ± SD PSV amplitude across eyes was 27.05 ± 3.41 mm/s, and the latencies ranged from 126 to 181 ms (Table 3). There was no difference between the eyes for IOP, PSV amplitude, R-MaxSlope and R-PSV½ (p-values 0.263-1.000). A very small but statistically significant inter-eye difference was observed for R-PSV (median difference 2 ms, $p = 0.041$). PSV amplitude and ECG-retina latencies were similar between the sexes, with no statistically significant differences (p-values 0.935–0.979). For full inter-eye and sex comparison data see Supplementary Tables S1 and S2.

ECG-retina latencies demonstrated weak-moderate negative correlations with age, with the strongest correlation observed between age and R-PSV½ ($\rho = -0.49$, $p = 0.015$). Heart rate was negatively correlated with all three ECG-retina latencies (ρ ranging − 0.43-(-0.44), p-values all < 0.05). Ocular perfusion pressure (OPP) measures showed weak correlations with ECG-retina latencies, with some associations approaching statistical significance. PSV showed no significant correlations with systemic variables or perfusion pressure measures. Full correlation coefficients and p-values are provided in Supplementary Table S3.

These analyses are exploratory and based on a small pilot cohort ($N = 25$). No multivariable adjustment was performed, and multiple comparison corrections were not applied. Consequently, these findings should be interpreted cautiously and primarily serve to generate hypotheses for future studies.

Discussion

Retinal vasculature, as a direct extension of the systemic circulation, offers a unique, non-invasive window into microcirculatory dynamics that mirror the health of the heart and brain. While previous research has linked ocular and cardiac blood flow, technological limitations have limited our ability to capture cardiac-resolved high-speed hemodynamics in real-time. To address this, we integrated a one-lead ECG with an LDH device, and developed custom synchronization software. This system creates a novel platform for cardiac-resolved dynamic retinal blood flow imaging, and provides high precision, quantitative measurements for the field of Oculomics. The aim of this study is to describe the development and validation of this combined LDH ECG system.

When assessing time and interference in a complex system, it is often difficult to isolate individual components' contributions to bias and measurement error. Here we present latency metrics defined as the time between the ECG R-peak and the appearance of systolic flow in the retinal circulation. This interval represents a composite timing metric reflecting the sequence from cardiac electrical activation and subsequent mechanical ejection, pulse propagation within the carotid-ophthalmic circulation, and arrival of flow at the retinal circulation. However, it is important to note that the current system does not allow quantification of the relative contributions of these individual components, and the resulting measure should therefore be interpreted as a composite timing metric.

The different latency metrics defined and used in this study represent alternative methods of detecting the same physiological transition within the LDH waveform, rather than distinct phenomena. Accordingly, differences between latency definitions primarily reflect feature-detection variability rather than separate vascular processes.

To verify accurate temporal alignment between the ECG and LDH signals, we evaluated three complementary aspects of timing: first, whether the two systems measure time consistently, referred to as "temporal stability"; second, whether the signals start simultaneously; and third, whether internal hardware introduces systematic latency. The following paragraphs describe these evaluations in detail.

To test temporal stability between the two systems, we compared the three LDH-derived beat-to-beat intervals with the ECG R-R intervals and found that they closely tracked each other, indicating consistent timing between the systems. While there was a statistically significant mean difference between the ECG R-R intervals and the MaxSlope and PSV½ intervals, the difference was small (~3 ms) relative to the mean R-R interval (761 ms), representing < 0.5% of the interval. For reference, the mean R-MaxSlope and R-PSV½ were ~127 ms - almost 40 times larger than the difference. The SD appears large relative to the mean difference, primarily reflecting the very small mean bias, but also potentially due to a combination of additional factors. First, physiological variability, such as beat-to-beat fluctuations in breathing, IOP, autonomic tone, pulse propagation, and microvascular dynamics, can alter the morphology and timing of LDH waveforms. Second, temporal resolution limitations of the LDH signal (effective resolution ~ 13.8 ms) introduce inherent uncertainty in timing estimation, although interpolation improves sub-frame precision. Third, comparing easily detectable peaks of an electrical signal with peaks of a fluid waveform, which are susceptible to morphological variability and physiological changes, introduces expected variability in feature timing and can produce timing jitter in feature

detection despite consistent temporal alignment between the two signals. This is supported by our findings that PSV, which is more morphology-dependent, exhibits higher variability (SD ~ 36 ms) compared to MaxSlope and PSV½ (SD ~ 21 ms), indicating that feature definition significantly impacts timing precision. The relative contributions of physiological versus methodological factors could not be quantified in this study, as reference measurements were not available to isolate each source. Future studies with higher LDH frame rate acquisition or morphology-robust feature definitions should help isolate and provide the ability to reduce specific sources of variability. Overall, the very small mean bias indicates that the two systems measure time consistently without temporal drift between the two signals, while the observed variability reflects a combination of physiological and methodological factors inherent to waveform-based feature extraction.

To align the signals and verify whether they start simultaneously, we used a common clock with centralized nanosecond-resolution Unix timestamping and performed a technical validation quantifying the offset between the two systems, showing an average offset of 1.17 ± 1.88 ms. For internal system latency, while we did not use an external trigger to directly measure it, the AD8232 ECG board has previously been shown to have an end-to-end latency under 3 ms[32]. Combined, these indicate that the total system offset is under 5 ms.

The temporal stability, minimal synchronization offset, and low internal hardware latency, together support the presence of accurate temporal alignment between the cardiac and retinal signals.

External validation of the temporal alignment is supported by our Mean R-MaxSlope of 126 ± 23 ms, which is comparable to heart-retina time (HRT) reported in a study coupling ECG to optical coherence tomography, where HRT was defined as the time from the R-wave peak to the sharpest rise of blood flow velocity, with a measured mean of 144 ± 19 ms[33]. The 18 ms difference may reflect differences between imaging modalities, as LDH provides a continuous blood flow waveform from which timing features are directly extracted, whereas OCT derives flow timing through additional processing steps, which may influence the detected timing of the systolic upstroke. Differences in study populations and use of different imaging modalities with fundamentally different optical and analytical mechanisms are also possible contributors. Nonetheless, both results are within a similar range, providing external validation to our findings.

In this pilot study, the ICCs of within-eye repeatability for the different ECG-retina latencies were moderate to strong (0.65–0.78), with low median CVs (4.8–6.0%). Among the three latencies examined, R-PSV½ had the highest ICC and the lowest CV, making it the most stable metric we examined, and suggesting this would be the most reliable metric for longitudinal and comparative studies. In contrast, timing based on the PSV peak showed greater variability, consistent with its sensitivity to waveform morphology. These results indicate this system provides repeatable measurements of cardiac cycle-resolved retinal blood flow, with R-PSV½ being the most robust latency metric.

We report for the first time mean ± SD for PSV amplitude and for the three latency metrics we defined. To our knowledge, these are the first quantitative values for LDH-derived metrics in a healthy cohort.

When comparing between the eyes, a small statistically significant difference was observed for R-PSV, however, the absolute magnitude of this difference was small, and no difference was observed for any of the other metrics. Given the modest sample size and multiple comparisons, this finding should be interpreted cautiously, as it may reflect statistical variability rather than a true physiological difference. Overall, these results support the use of either eye for future studies, in healthy control subjects.

No statistically significant differences between sexes were seen for PSV amplitude and ECG-retina latencies, despite higher OPP in males. ECG-retina latencies showed moderate associations with age and heart rate, but no significant association with OPP in healthy adults. PSV amplitude was not associated with systemic variables or OPP. Overall, these findings may reflect the presence of autoregulatory mechanisms that help maintain relatively stable retinal blood flow across the physiological range of OPP in healthy subjects.

LDH joins and complements existing non-invasive arterial waveform assessment techniques that reflect a growing interest in capturing cardiovascular dynamics across scales. For example, handheld optical systems have been developed to measure carotid pulse waveforms for non-invasive evaluation of cardiovascular and arterial health, while ultrasound-based approaches enable non-invasive estimation of carotid arterial pressure waveforms during physiological stress[34,35]. In addition, laser speckle-based technologies have been adapted into both device-based and wearable formats, including endoscopic systems for tissue-level blood flow visualization and wearable flowmetry systems for continuous monitoring of cerebral perfusion[36,37]. While these technologies demonstrate increasing portability and clinical feasibility, most focus on large-vessel or regional perfusion measurements and typically provide limited spatial resolution of individual microvascular flow dynamics.

Within this group, some approaches incorporate ECG synchronization to align cardiac electrical activity with vascular signals, and a subset derives pulse arrival time (PAT), a metric describing the interval between cardiac electrical activation and peripheral pulse detection[38]. Conceptually, the ECG-retina latencies in our study are similar to PAT, although the terminal measurement reflects retinal microvascular flow rather than peripheral arterial waveform arrival. The ECG-retina latency observed in this study (~ 127 ms) falls within the range of reported PAT values (approximately 126 ms at the ear and 269 ms at the finger), supporting its conceptual similarity[39].

Among biomarkers, PAT has been explored for assessing cardiovascular health, including arterial stiffness assessment and risk stratification[38,40–43] The present ECG-synchronized LDH platform extends the concept of PAT to a system that provides direct visualization of microvascular hemodynamics with high temporal and spatial resolution. This distinguishes LDH from peripheral waveform-based approaches, which generally infer vascular properties indirectly from distal pulse detection. While the translational implications of these retinal timing metrics remain to be established, they provide a foundation for future studies in conditions associated with altered ocular hemodynamics. This includes ophthalmic conditions including glaucoma, diabetic retinopathy, and age-related macular degeneration, as well as broader systemic applications in Oculomics.

This study has several limitations to acknowledge. The relatively small sample size and inclusion of only healthy subjects, while sufficient for system validation and assessment of repeatability, limit the generalizability of findings and the ability to detect small differences. Additionally, we demonstrate here repeatability in a single imaging session, and did not examine reproducibility over multiple visits. The reported correlations between ECG-retina latency metrics and age or heart rate are exploratory; the small sample size and absence of adjustment or multiple comparison correction limit the strength of these associations, which should be confirmed in larger studies. Image and waveform quality were assessed through manual review by a single grader; future work could focus on developing standardized automated quality-control approaches to reduce reliance on manual grading and improve reproducibility in larger datasets. Additionally, each LDH recording lasted 3.5 s, the only currently available recording length. This window captures multiple cardiac cycles but may not fully reflect beat-to-beat variability or longer-term hemodynamics, limiting repeatability estimates and physiological interpretations to the observed time window. Finally, we did not use an external hardware trigger to test internal system latency, however, the AD8232 ECG board has a previously reported end-to-end latency under 3 ms. In addition, we measured a synchronization offset of 1.17 ± 1.88 ms. Combined, these contribute a negligible offset compared to the measured biological ECG-retina latencies (~ 127 ms), providing sufficient resolution for capturing eye-heart hemodynamics.

Future directions include focusing on additional LDH-derived metrics not examined in this study, such as venous velocity, flow volume measures, and frequency-domain features. The ECG-based temporal alignment provides a platform to couple the LDH data with other ECG-gated devices such as echocardiogram, even if acquisitions are performed on different days or in different locations - facilitating multimodal studies of the eye-heart relationship. In addition, LDH could be synchronized with other temporally resolved physiologic signals, such as electroencephalography. Extending acquisition beyond 3.5 s would allow assessment of beat-to-beat variability, respiratory influences, and a more complete characterization of ocular hemodynamics.

Conclusions

In summary, we have developed and validated a novel platform that integrates ECG with LDH to achieve cardiac cycle-resolved retinal blood flow measurements. Our results show that the system reliably synchronizes cardiac and retinal signals, and provides repeatable metrics of real-time hemodynamics, with R-PSV½ emerging as the most robust ECG-retina latency. Furthermore, this study provides preliminary normative data for healthy adults and demonstrates that retinal blood flow is relatively preserved across a physiological range of ocular perfusion pressure. This integrated ECG-LDH platform offers a new approach for exploring the eye-heart relationship, with potential applications in both clinical and research settings.

Data availability

The datasets generated and analyzed during the current study are available from the corresponding author on reasonable request. All key findings and summarized data supporting the results of this study are included in this published article and its supplementary files.

Code availability

The custom MATLAB scripts used are available from the corresponding author upon reasonable request.

Received: 14 January 2026; Accepted: 25 April 2026
Published online: 03 May 2026

References

1. Patton, N. et al. Retinal vascular image analysis as a potential screening tool for cerebrovascular disease: a rationale based on homology between cerebral and retinal microvasculatures. *J. Anat.* **206** (4), 319–348. https://doi.org/10.1111/j.1469-7580.2005.00395.x (2005).
2. Cheung, C. Y., Ikram, M. K., Sabanayagam, C. & Wong, T. Y. Retinal microvasculature as a model to study the manifestations of hypertension. *Hypertens. Dallas Tex. 1979.* **60** (5), 1094–1103. https://doi.org/10.1161/HYPERTENSIONAHA.111.189142 (2012).
3. Cabrera DeBuc, D., Somfai, G. M. & Koller, A. Retinal microvascular network alterations: potential biomarkers of cerebrovascular and neural diseases. *Am. J. Physiol. - Heart Circ. Physiol.* **312** (2), H201–H212. https://doi.org/10.1152/ajpheart.00201.2016 (2017).
4. Wang, B. et al. Effect of Intensive Blood Pressure Lowering Treatment on Retinal Microvasculature: Secondary Analysis From ESPRIT. *J. Am. Coll. Cardiol.* **86** (17), 1377–1388. https://doi.org/10.1016/j.jacc.2025.05.020 (2025).
5. Kellner, R. L. et al. The Eye as the Window to the Heart: Optical Coherence Tomography Angiography Biomarkers as Indicators of Cardiovascular Disease. *J. Clin. Med.* **13** (3), 829. https://doi.org/10.3390/jcm13030829 (2024).
6. Alarcon-Martinez, L. et al. Neurovascular dysfunction in glaucoma. *Prog Retin Eye Res.* **97**, 101217. https://doi.org/10.1016/j.preteyeres.2023.101217 (2023).
7. Moore, D., Harris, A., Wudunn, D., Kheradiya, N. & Siesky, B. Dysfunctional regulation of ocular blood flow: A risk factor for glaucoma? *Clin. Ophthalmol. Auckl. NZ.* **2** (4), 849–861. https://doi.org/10.2147/opth.s2774 (2008).
8. Taylor, T. R. P., Menten, M. J., Rueckert, D., Sivaprasad, S. & Lotery, A. J. The role of the retinal vasculature in age-related macular degeneration: a spotlight on OCTA. *Eye* **38** (3), 442–449. https://doi.org/10.1038/s41433-023-02721-7 (2024).
9. Pemp, B. & Schmetterer, L. Ocular blood flow in diabetes and age-related macular degeneration. *Can. J. Ophthalmol. J. Can. Ophtalmol.* **43** (3), 295–301. https://doi.org/10.3129/i08-049 (2008).
10. Linton, E. F. et al. Laser Speckle Flowgraphy Reveals Widespread Reductions in Ocular Blood Flow in nonexudative Age-Related Macular Degeneration. *Am. J. Ophthalmol.* **273**, 92–106. https://doi.org/10.1016/j.ajo.2025.01.012 (2025).
11. Nippert, A. R. & Newman, E. A. Regulation of blood flow in diabetic retinopathy. *Vis. Neurosci.* **37**, E004. https://doi.org/10.1017/S0952523820000036 (2020).
12. Harris, A. et al. Ocular blood flow as a clinical observation: Value, limitations and data analysis. *Prog Retin Eye Res Published online January*. **24**, 100841. https://doi.org/10.1016/j.preteyeres.2020.100841 (2020).
13. World Glaucoma Association » Consensus 6. https://wga.one/consensus/consensus-6/ (Accessed 6 January 2026).

14. Oculomics Current concepts and evidence - ScienceDirect. https://www.sciencedirect.com/science/article/pii/S1350946225000230 (Accessed 11 December 2025).
15. Honavar, S. G. Oculomics - The eyes talk a great deal. *Indian J. Ophthalmol.* **70** (3), 713. https://doi.org/10.4103/ijo.IJO_474_22 (2022).
16. Chaikijurajai, T., Ehlers, J. P. & Tang, W. H. W. Retinal Microvasculature: A Potential Window Into Heart Failure Prevention. *JACC Heart Fail.* **10** (11), 785–791. https://doi.org/10.1016/j.jchf.2022.07.004 (2022).
17. Zekavat, S. M. et al. Deep Learning of the Retina Enables Phenome- and Genome-Wide Analyses of the Microvasculature. *Circulation* **145** (2), 134–150. https://doi.org/10.1161/CIRCULATIONAHA.121.057709 (2022).
18. Wagner, S. K. et al. Insights into Systemic Disease through Retinal Imaging-Based Oculomics. *Transl Vis. Sci. Technol.* **9** (2), 6. https://doi.org/10.1167/tvst.9.2.6 (2020).
19. Ghenciu, L. A. et al. Retinal Imaging-Based Oculomics: Artificial Intelligence as a Tool in the Diagnosis of Cardiovascular and Metabolic Diseases. *Biomedicines* **12** (9), 2150. https://doi.org/10.3390/biomedicines12092150 (2024).
20. Lin, T. Y. et al. Individual Prognostication of Disease Activity and Disability Worsening in Multiple Sclerosis With Retinal Layer Thickness z Scores. *Neurol. Neuroimmunol. Neuroinflammation*. **11** (5), e200269. https://doi.org/10.1212/NXI.0000000000200269 (2024).
21. Suh, A. et al. Retina Oculomics in Neurodegenerative Disease. *Ann. Biomed. Eng.* **51** (12), 2708–2721. https://doi.org/10.1007/s10439-023-03365-0 (2023).
22. Dimitrova, G. & Kato, S. Color Doppler Imaging of Retinal Diseases. *Surv. Ophthalmol.* **55** (3), 193–214. https://doi.org/10.1016/j.survophthal.2009.06.010 (2010).
23. Dellafiore, C. et al. Reproducibility of retrobulbar blood flow velocity measurements in normal subjects using two different CDI devices. *Radiol. Med. (Torino)*. **120** (8), 737–744. https://doi.org/10.1007/s11547-015-0522-4 (2015).
24. Spaide, R. F., Fujimoto, J. G., Waheed, N. K., Sadda, S. R. & Staurenghi, G. Optical coherence tomography angiography. *Prog Retin Eye Res.* **64**, 1–55. https://doi.org/10.1016/j.preteyeres.2017.11.003 (2018).
25. Chalam, K. V. & Sambhav, K. Optical Coherence Tomography Angiography in Retinal Diseases. *J. Ophthalmic Vis. Res.* **11** (1), 84–92. https://doi.org/10.4103/2008-322X.180709 (2016).
26. Qureshi, M. M. et al. Advances in laser speckle imaging: From qualitative to quantitative hemodynamic assessment. *J. Biophotonics.* **17** (1), e202300126. https://doi.org/10.1002/jbio.202300126 (2024).
27. Puyo, L., Paques, M., Fink, M., Sahel, J. A. & Atlan, M. In vivo laser Doppler holography of the human retina. *Biomed. Opt. Express.* **9** (9), 4113–4129. https://doi.org/10.1364/BOE.9.004113 (2018).
28. Pellizzari, M. et al. High speed optical holography of retinal blood flow. *Opt. Lett.* **41** (15), 3503–3506. https://doi.org/10.1364/OL.41.003503 (2016).
29. Magnain, C. et al. Holographic laser Doppler imaging of microvascular blood flow. *JOSA* **31** (1), 2723–2735. https://doi.org/10.1364/JOSAA.31.002723 (2014).
30. Holographic laser Doppler ophthalmoscopy. https://opg.optica.org/ol/abstract.cfm?uri=ol-35-12-1941 (Accessed 12 December 2025).
31. Trihan, J. E. et al. Arterial Blood-Flow Acceleration Time on Doppler Ultrasound Waveforms: What Are We Talking About? *J. Clin. Med.* **12** (3), 1097. https://doi.org/10.3390/jcm12031097 (2023).
32. Inafuco, A. T. P., Machoski, P., Campos, D. P., Pichorim, S. F. & Mendes Junior, J. J. A. MOT: A Low-Latency, Multichannel Wireless Surface Electromyography Acquisition System Based on the AD8232 Front-End. *Sensors* **25** (12), 3600. https://doi.org/10.3390/s25123600 (2025).
33. Valmaggia, P. et al. Heart-retina time analysis using electrocardiogram-coupled time-resolved dynamic optical coherence tomography. *Sci. Rep.* **15** (1), 385. https://doi.org/10.1038/s41598-024-84417-w (2025).
34. Rinderknecht, D., De Balasy, J. M. & Pahlevan, N. M. A wireless optical handheld device for carotid waveform measurement and its validation in a clinical study. *Physiol. Meas.* **41** (5), 055008. https://doi.org/10.1088/1361-6579/ab7b3f (2020).
35. Seo, J., Lee, H. S. & Sodini, C. G. Non-Invasive Evaluation of a Carotid Arterial Pressure Waveform Using Motion-Tolerant Ultrasound Measurements During the Valsalva Maneuver. *IEEE J. Biomed. Health Inf.* **25** (1), 163–174. https://doi.org/10.1109/JBHI.2020.2995344 (2021).
36. Kim, Y., Choi, W. J., Oh, J. & Kim, J. K. Compact Smartphone-Based Laser Speckle Contrast Imaging Endoscope Device for Point-of-Care Blood Flow Monitoring. *Biosensors* **12** (6), 398. https://doi.org/10.3390/bios12060398 (2022).
37. Yeo, C. et al. An affordable, wearable, fiber-free pulsed-mode diffuse speckle contrast flowmetry (PM-DSCF) sensor for noninvasive measurements of deep cerebral blood flow. https://arXiv.org/abs/2502.08000v1. (2025).
38. Deshmukh, C. A., Jindal, G. D., Bagal, U. R. & Nagare, G. D. Pulse arrival time: Measurement and clinical applications. *MGM J. Med. Sci.* **9** (1), 103. https://doi.org/10.4103/mgmj.mgmj_23_22 (2022).
39. Block, R. C. et al. Conventional pulse transit times as markers of blood pressure changes in humans. *Sci. Rep.* **10** (1), 16373. https://doi.org/10.1038/s41598-020-73143-8 (2020).
40. Kwon, Y. et al. Pulse Arrival Time, a Novel Sleep Cardiovascular Marker: the Multi-Ethnic Study of Atherosclerosis. *Thorax* **76** (11), 1124–1130. https://doi.org/10.1136/thoraxjnl-2020-216399 (2021).
41. Paliakaitė, B., Daukantas, S. & Marozas, V. Assessment of pulse arrival time for arterial stiffness monitoring on body composition scales. *Comput. Biol. Med.* **85**, 135–142. https://doi.org/10.1016/j.compbiomed.2016.04.012 (2017).
42. Haidour, N. et al. Multi-lens ultrasound arrays enable large scale three-dimensional micro-vascularization characterization over whole organs. *Nat. Commun.* **16** (1), 9317. https://doi.org/10.1038/s41467-025-64911-z (2025).
43. Cinquino, M. et al. Enhancing cardiovascular health monitoring: Simultaneous multi-artery cardiac markers recording with flexible and bio-compatible AlN piezoelectric sensors. *Biosens. Bioelectron.* **267**, 116790. https://doi.org/10.1016/j.bios.2024.116790 (2025).

Author contributions

K.W. and A.H. conceived the study. K.W. led the integration of the ECG-LDH platform, developed the LDH metrics and timing analysis methodology, performed clinical imaging and statistical analysis, and drafted the manuscript. N.S. and L.M. designed the hardware and synchronization software. Y.L. and M.A. assisted with system development. B.A.S., A.V.V., L.A.G., and S.P. contributed to recruitment and manuscript preparation. G.G. and T.Y.P.C. reviewed the manuscript. R.R. provided mentorship and reviewed the manuscript. A.H. supervised the project, provided mentorship and reviewed the manuscript. All authors reviewed the final manuscript.

Funding

Alon Harris is supported by NIH grant R01EY034718, NYEE Foundation grants, The Glaucoma Foundation, and in part by a Challenge Grant award from Research to Prevent Blindness, NY. Alon Harris is supported by the Barry Family Center for Ophthalmic Artificial Intelligence & Human Health. Alice Verticchio Vercellin is supported by a NYEE Foundation grant. Giovanna Guidoboni is supported by NIH R01EY034718 and NSF 2412130.

Declarations

Competing interests
The authors declare no competing interests.

Commercial relationships disclosure
Professor Alon Harris would like to disclose that he received remuneration from AdOM, Qlaris, and Cipla for serving as a consultant, and he serves on the board of AdOM, Qlaris and SlitLed. Professor Alon Harris holds an ownership interest in AdOM, Oxymap, Qlaris, SlitLed, and AEYE Health. Alice Verticchio Vercellin is an external collaborator of the IRCCS Fondazione Bietti, Rome. If you have questions regarding paid relationships that your physician/researcher may have with industry, you are encouraged to talk with your physician/researcher or check for industry relationships posted on individual faculty pages on our website athttp://icahn.mssm.edu.

Additional information
Supplementary Information The online version contains supplementary material available at https://doi.org/10.1038/s41598-026-51137-2.

Correspondence and requests for materials should be addressed to A.H.

Reprints and permissions information is available at www.nature.com/reprints.

Publisher's note Springer Nature remains neutral with regard to jurisdictional claims in published maps and institutional affiliations.